Title no. 110-M36

Simplified Diverse Embedment Model for Steel Fiber-Reinforced Concrete Elements in Tension

by Seong-Cheol Lee, Jae-Yeol Cho, and Frank J. Vecchio

A simplified version of the Diverse Embedment Model (DEM) for steel fiber-reinforced concrete (SFRC) is derived by eliminating the double numerical integration, which complicates the calculation procedure of the DEM. To simplify the DEM, fiber slip on the longer embedded side is not considered in the calculation of the fiber tensile stress at a crack, while coefficients for frictional bond behavior and mechanical anchorage effect are incorporated to prevent overestimation of the tensile stress attained by fibers. The tensile stress behavior of SFRC predicted by the Simplified DEM (SDEM) shows good agreement with that obtained from the DEM; hence, the model's accuracy has largely been retained despite the simplification. In comparisons with test results reported in the previous literature, the SDEM is shown to simulate not only the direct tensile behavior but also the flexural behavior of SFRC members. The SDEM can easily be implemented in currently available analysis models so that it can be useful in the modeling of structural behavior of SFRC members or structures.

INTRODUCTION

It is well-known that, unlike normal concrete, steel fiber-reinforced concrete (SFRC) members typically demonstrate a ductile post-cracking behavior due to the steel fibers bridging the cracks. With this beneficial aspect of SFRC, many researchers[1-4] have conducted theoretical or experimental investigations into the practical use of SFRC in structural members subjected to various loading conditions. However, although the structural behavior of SFRC members subjected to tension has been experimentally studied by many researchers, the practical application of SFRC in actual construction is still muted. One reason for this is that most research efforts have mainly focused on qualitative evaluations for the tensile behavior of SFRC members[5-9] rather than on the development of a rational model that can be easily employed to predict the structural behavior of SFRC members. In addition, the tensile behavior of SFRC members is dominated by the pullout behavior of each single fiber bridging a crack which, in turn, is affected by the steel fiber type. The influence of steel fiber type on the tensile behavior can clearly be seen in Fig. 1, in which the post-cracking tensile stresses are normalized by the peak tensile stress after initial cracking. As shown in this figure, the SFRC member with hooked-end fibers shows a steeper decrease of the post-cracking tensile stress response due to straightened or fractured end hooks and deterioration of concrete in the vicinity of the fiber.[10]

Several researchers have made contributions to the development of rational models for calculating the tensile behavior of SFRC members; some of the more influential works are summarized in Table 1. By assuming that the number of fibers bridging a crack decreases linearly with increasing
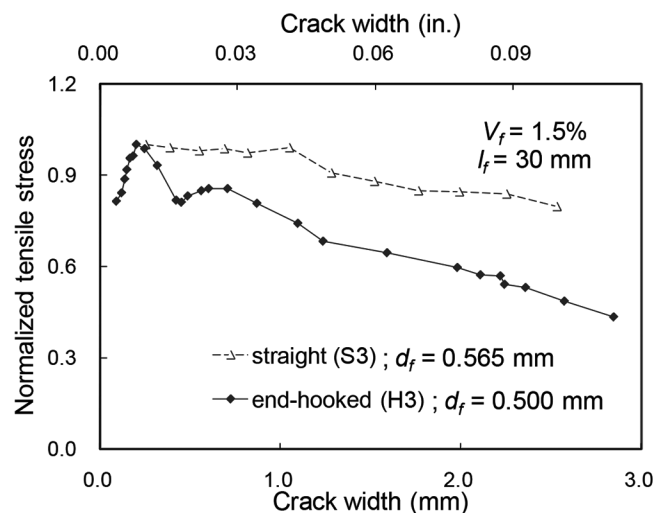

Fig. 1—Normalized tensile behavior of SFRC members in tension tested by Lim et al.[6] (1 mm = 0.0394 in.)

crack width, Marti et al.[11] developed a simple formula that describes a relationship between crack width and tensile stress. Later, introducing an engagement factor to consider the effect of fiber inclination angle on fiber pullout behavior, Voo and Foster[12] developed the Variable Engagement Model (VEM), in which the random distribution of fibers in a three-dimensional (3-D) infinite element was taken into account. However, the appropriateness of these two models for SFRC members with hooked-end fibers is questionable because a uniform bond stress along a fiber was assumed. Leutbecher and Fehling[13] presented a model that considers the effect of fibers on crack widths in SFRC members with conventional reinforcing bars, but this model also assumed an average bond stress between the fiber and matrix and mainly focused on members with straight steel fibers. Stroeven[14] developed a formulation that considered varying uniform bond stress along a fiber according to the fiber type; the slope for the descending branch in the relationship between tensile stress and crack width was adjusted to the fiber type. Recently, Lee et al.[15,16] proposed the Diverse Embedment Model (DEM), in which the tensile stresses due to the frictional bond behavior and the mechanical anchorage effect were separately evaluated from the pullout behavior of a single straight fiber or hooked-end fiber.

ACI member **Seong-Cheol Lee** *is an Assistant Professor at KINGS, Ulsan, South Korea. He received his PhD from Seoul National University, Seoul, South Korea, in 2007. His research interests include the shear behavior of concrete structures and the analysis of prestressed concrete structures and fiber-reinforced concrete members.*

ACI member **Jae-Yeol Cho** *is an Associate Professor in the Department of Civil & Environmental Engineering at Seoul National University. He received his PhD from Seoul National University. His research interests include nonlinear analysis and optimized design of reinforced and prestressed concrete structures, material modeling, and similitude laws for dynamic tests of concrete structures.*

Frank J. Vecchio, *FACI, is a Professor in the Department of Civil Engineering at the University of Toronto, Toronto, ON, Canada. He is a member of Joint ACI-ASCE Committees 441, Reinforced Concrete Columns, and 447, Finite Element Analysis of Reinforced Concrete Structures. His research interests include nonlinear analysis and design of reinforced concrete structures, constitutive modeling, performance assessment and forensic investigation, and repair and rehabilitation of structures.*

Figure 2 compares the responses calculated from the various models against results from a test conducted by Susetyo[17] in which hooked-end steel fibers were used. It can be seen that the DEM provides the closest correlation to the test results, particularly for the rapid decrease in the tensile stress. Similar trends and correlations were seen with other specimens tested by several researchers[6,17,18]; refer to the Appendix*, in which comparison results are presented

*The Appendix is available at **www.concrete.org** in PDF format as an addendum to the published paper. It is also available in hard copy from ACI headquarters for a fee equal to the cost of reproduction plus handling at the time of the request.

for 18 SFRC specimens. In the DEM, however, one must undertake a double numerical integration to calculate the average tensile stress of steel fibers at a crack. This complicates the implementation of the DEM into various analysis models[19-22] and programs[23,24] useful for the calculation of the structural behavior of SFRC members with or without conventional reinforcing bars.
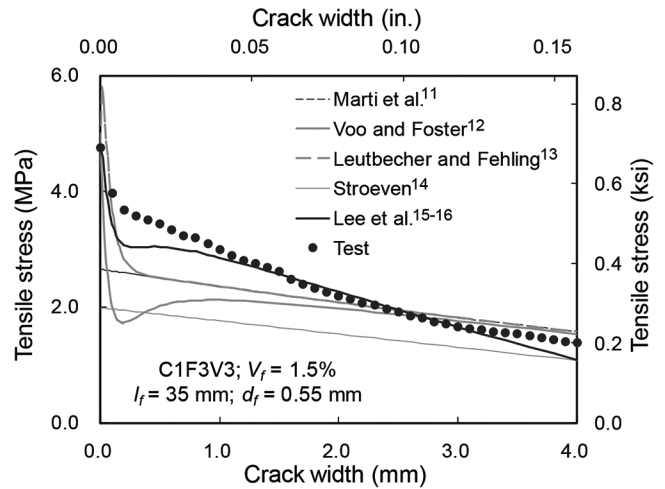
Fig. 2—Comparison of various models for SFRC members in tension. (Note: 1 mm = 0.0394 in.)

Table 1—Models for SFRC members in tension

Researcher	Model
Marti et al.[11]	$$f_f = \frac{V_f l_f \tau_b}{2d_f}\left(1 - \frac{2w_{cr}}{l_f}\right)^2$$
Voo and Foster[12] (VEM)*	$$f_f = \frac{V_f l_f \tau_b}{d_f}\frac{\tan^{-1}\left(w_{cr}/\alpha\right)}{\pi}\left(1 - \frac{2w_{cr}}{l_f}\right)^2$$ where $\alpha = d_f/3.5$
Leutbecher and Fehling[13]*	$$f_f = \sigma_{cf0}\left(2\sqrt{\frac{w_{cr}}{w_0}} - \frac{w_{cr}}{w_0}\right) \text{ for phase of fiber activation}$$ $$f_f = \sigma_{cf0}\left(1 - 2\frac{w_{cr}}{l_f}\right)^2 \text{ for phase of fiber pullout}$$ where $w_0 = \frac{\tau_{fm}l_f^2}{E_f d_f}$; $\sigma_{cf0} = \eta g \frac{V_f l_f \tau_b}{d_f}$; and η and g are coefficients for orientation and efficiency of fibers, respectively.
Stroeven[14]	$$f_f(x) = \frac{1}{3}\frac{l_f}{d_f}V_f\tau_b\left(1 + \frac{1}{2}\omega_2\right)\left(1 - k\frac{w_{cr}}{l_f}\right)$$ $$f_f(z) = \frac{1}{3}\frac{l_f}{d_f}V_f\tau_b\left(1 - \omega_2\right)\left(1 - k\frac{w_{cr}}{l_f}\right)$$ where ω_2 is degrees of planar fiber orientation; and $k = 8$ or 4 for a straight or hooked-end fiber, respectively.
Lee et al.[15,16] (DEM)*	$$f_f = \alpha_f V_f \sigma_{f,cr,avg}$$ where $\sigma_{f,cr,avg} = \frac{2}{l_f}\int_0^{l_f/2}\int_0^{\pi/2}\sigma_{f,cr}(l_a,\theta)\sin\theta d\theta dl_a$; and $\sigma_{f,cr}$ is fiber tensile stress at a crack.

*In these models, tensile stress due to tension softening of concrete matrix should be added.

A simplified version of the DEM can be formulated by eliminating the double numerical integration and replacing it with easily determined coefficients. Thus, the Simplified Diverse Embedment Model (SDEM) is more amenable to practical applications without significant loss of accuracy.

RESEARCH SIGNIFICANCE

In this paper, the SDEM has been derived to predict the crack width-tensile stress behavior of SFRC members subjected to direct tension. The double numerical integration required by the DEM has been eliminated, while the accuracy has been preserved. Thus, the SDEM can be more easily implemented into existing models[19-22] or programs[23,24] for the analysis of SFRC members or structures. Consequently, the SDEM can be useful in the prediction of SFRC members with or without conventional reinforcing bars subjected to not only uniaxial tension but also various loading conditions because tensile stress attained by fibers are considerable not only under service load but also at failure.

DERIVATION OF SDEM
Fundamental assumption for SDEM

Within the DEM formulation, the pullout behavior of a single fiber embedded on both sides is simplified by considering it to be a rigid-body translation, in which both the elongation of the fiber and the variation of slip along the fiber are neglected. With this simplification, the pullout behavior of a single fiber embedded on both sides can be analyzed in regard to three conditions: equilibrium, constitutive behavior, and compatibility. The equilibrium condition is that the fiber tensile stress at a crack calculated from the shorter embedded side should be the same as that from the longer embedded side. For the constitutive response, the frictional bond behavior and mechanical anchorage effect are considered separately in the fiber slip and tensile stress relationships, taking into account the effect of the fiber inclination angle. The compatibility requirement is that the crack width be equal to the sum of the slips on both sides. However, the compatibility condition makes the calculation of the fiber tensile stress at a crack complicated because an iteration procedure is required for the calculation of the slip on either side. This compatibility, consequently, makes a double numerical integration inevitable in the calculation of the average fiber tensile stress at a crack, as presented in Table 1.

To simplify the DEM, one more assumption can be made with respect to compatibility: the crack width can be assumed to be the same as the slip on the shorter embedded side, while the slip on the longer embedded side is neglected. With this assumption, the iteration procedure required to analyze the pullout behavior of a single fiber embedded on both sides can be omitted so that the double numerical integration in the DEM can be averted. However, the effect of fiber slip of the longer embedded side on the fiber tensile stress at a crack can be significant in some cases. Hence, in this paper, two coefficients will be introduced within the formulation to compensate for the relaxed compatibility condition. The details follow.

Model derivation for frictional bond behavior

In the case of straight fibers, because it is assumed that the slip of a fiber occurs only on the shorter embedded side, a fiber tensile stress at a crack can be calculated by integrating the frictional bond stress along the shorter embedment part
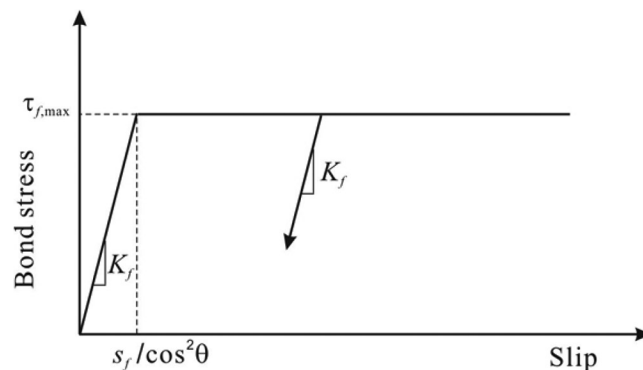

Fig. 3—Frictional bond behavior of single fiber.

of the fiber. In this paper, a bilinear relationship between the bond stress and slip is employed for the frictional bond behavior of a fiber, as illustrated in Fig. 3, which considers the effect of the fiber inclination angle on the frictional bond behavior. The frictional bond strength is constant, while the slip at the peak increases with an increase of the fiber inclination angle, as assumed in the DEM based on test results reported by Banthia and Trottier.[25] Note that the slip reported in the figure is the same as the crack width because the slip of a fiber on the longer embedded side is neglected.

Because a bilinear relationship is employed for the frictional bond behavior of fibers, two phases of response should be considered in the calculation of the fiber tensile stress at a crack. The first occurs when the crack width is so small that all fibers are still on the linearly ascending part of the constitutive law for the frictional bond behavior; the second prevails when the crack width is sufficiently large such that some fibers exhibit plastic frictional bond behavior, while other fibers remain in the pre-peak regime.

Without suitable compensation made, the fiber tensile stress can be significantly overestimated when the fiber slip on the longer embedded side is neglected, particularly for a fiber that does not reach the frictional bond strength. For example, consider a situation where the crack width is $0.60s_f$; the fiber is perpendicular to the crack surface; and the shorter and longer embedment lengths are $0.25l_f$ and $0.75l_f$, respectively. In this case, the calculated frictional bond stress on the shorter embedded side is $0.60\tau_{f,max}$, as determined from the frictional bond behavior presented in Fig. 3 with the fiber slip on the longer embedded side neglected. This frictional bond stress is significantly larger than the $0.45\tau_{f,max}$ value that would be calculated if the fiber slip on the longer embedded side was considered. The effect of a fiber slip on the longer embedded side quickly diminishes after a fiber reaches the frictional bond strength because the slip on the longer embedded side decreases as the fiber tensile stress decreases with an increase in the crack width. Therefore, to consider the effect of slip of the fiber on the longer embedded side on the frictional bond stress of a fiber, a factor β_f will be applied to fibers not having reached the frictional bond strength when the average frictional bond stress or the average fiber tensile stress is calculated.

For the first phase of response, in which the crack width is smaller than the slip s_f corresponding to the initiation of plastic frictional bond behavior of a fiber perpendicular to the crack surface, the average frictional bond stress considering the random distribution of the fiber inclination angle illustrated in Fig. 4 can be calculated as Eq. (1)
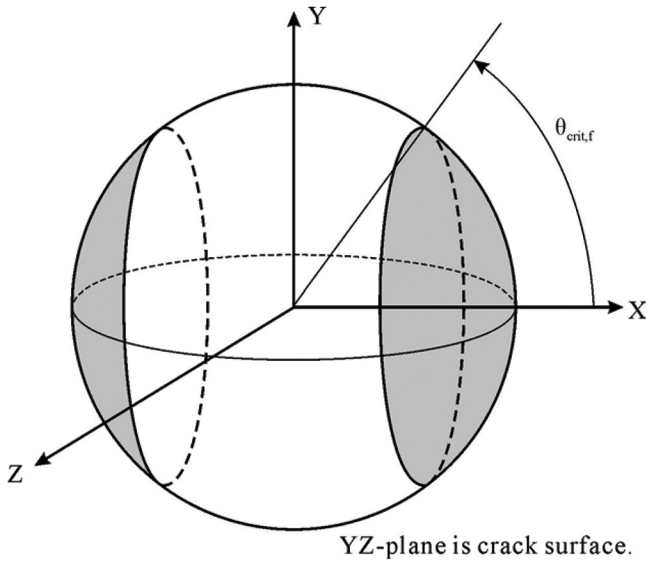
Fig. 4—Probability of fiber inclination angle using sphere representation.[12]
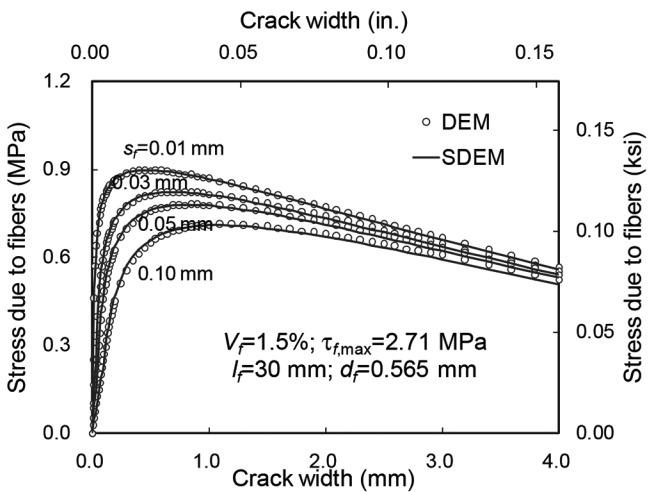

Fig. 5—Comparison of SDEM with DEM for tensile stress attained by straight fibers. (Note: 1 MPa = 145 psi; 1 mm = 0.0394 in.)

$$\tau_{f,avg} = \beta_f \frac{2\pi \int_0^{\pi/2} \frac{w_{cr}}{w_{p\theta,f}} \tau_{f,max} \sin\theta d\theta}{2\pi}$$

$$= \frac{\beta_f}{3} \frac{w_{cr}}{s_f} \tau_{f,max} \quad \text{for } w_{cr} < s_f \tag{1}$$

where $w_{p\theta,f}$ is the crack width at the initiation of plastic frictional bond behavior of a fiber with an inclination angle of θ, calculated as $w_{p\theta,f} = s_f/\cos^2\theta$; and β_f is a coefficient reflecting the effect of fiber slip on the longer embedded side. From comparisons between the average fiber tensile stresses calculated by the DEM and the simplified procedure, it has been analytically determined that $\beta_f = 0.67$.

For the second phase of response, giving consideration to the effect of the fiber inclination angle on the frictional bond behavior, the critical fiber inclination angle corresponding to the crack width w_{cr} at the initiation of plastic frictional bond behavior can be derived as Eq. (2)

$$\theta_{crit,f} = \cos^{-1}\left(\sqrt{s_f/w_{cr}}\right) \text{ for } w_{cr} \geq s_f \tag{2}$$

In the same manner as for the first phase, the average frictional bond stress considering the random distribution of the fiber inclination angle can be derived for the second phase as Eq. (3)

$$\tau_{f,avg} = \frac{2\pi \int_0^{\theta_{crit,f}} \tau_{f,max} \sin\theta d\theta}{2\pi} + \beta_f \frac{2\pi \int_{\theta_{crit,f}}^{\pi/2} \frac{w_{cr}}{w_{p\theta,f}} \tau_{f,max} \sin\theta d\theta}{2\pi}$$

$$= \left(1 - \sqrt{\frac{s_f}{w_{cr}}} + \frac{\beta_f}{3}\sqrt{\frac{s_f}{w_{cr}}}\right)\tau_{f,max} \text{ for } w_{cr} \geq s_f \tag{3}$$

Assuming that the probability density for the shorter embedment length of a fiber is uniform at initial cracking, the average fiber tensile stress at a crack due to the frictional bond behavior can be calculated by integrating the average bond stress along a fiber as Eq. (4)

$$\sigma_{f,cr,st} = \tau_{f,avg} \frac{l_f}{d_f}\left(1 - \frac{2w_{cr}}{l_f}\right)^2 \tag{4}$$

Because the number of fibers bridging a crack surface per unit area is $\alpha_f V_f/A_f$,[26] the tensile stress of an SFRC element due to the frictional bond behavior can be calculated as Eq. (5)

$$f_{st} = \alpha_f V_f \sigma_{f,cr,st} = \alpha_f V_f K_{st} \tau_{f,max} \frac{l_f}{d_f}\left(1 - \frac{2w_{cr}}{l_f}\right)^2 \tag{5}$$

where $K_{st} = \begin{cases} \dfrac{\beta_f}{3}\dfrac{w_{cr}}{s_f} & \text{for } w_{cr} < s_f \\[2ex] 1 - \sqrt{\dfrac{s_f}{w_{cr}}} + \dfrac{\beta_f}{3}\sqrt{\dfrac{s_f}{w_{cr}}} & \text{for } w_{cr} \geq s_f \end{cases}$

In Eq. (5), α_f can be assumed to be 0.5 for a 3-D infinite element, which can be used for general SFRC structures in which the dimensions are much larger than the fiber length.

In Fig. 5, the tensile stresses attained by straight fibers, as calculated by the SDEM according to Eq. (5), are compared with those predicted by the DEM. It can be seen that tensile stresses calculated by the simplified model show good agreement with those determined from the more rigorous DEM, regardless of the variation of s_f.

Model derivation for mechanical anchorage effect

In the case of hooked-end fibers, the effect of mechanical anchorage on the pullout behavior should be considered in addition to the frictional bond behavior. From the test results presented by Banthia and Trottier,[25] the effect of the fiber inclination angle on the mechanical anchorage effect can be assumed to be the same as for straight fibers; the maximum force due to the mechanical anchorage is constant, while the

slip at the peak increases with an increase in the fiber inclination angle. Based on the work of Sujivorakul et al.,[27] the relationship between fiber slip and tensile force provided by the mechanical anchorage is idealized with parabolic and linear relationships for the pre- and post-peak behaviors, respectively, with consideration of the fiber inclination angle effect, as illustrated in Fig. 6.[15]

Similar to the frictional bond behavior, three phases can be considered in the calculation of the fiber tensile stress due to mechanical anchorage: pre-peak, post-peak, and full deterioration of the end hook, as illustrated in Fig. 6. When the crack width is smaller than s_{eh}, all mechanical anchorages follow the pre-peak tensile behavior. Therefore, through the same procedure presented in Eq. (1), the average tensile force due to mechanical anchorage can be calculated with consideration given to the random distribution of the fiber inclination angle as Eq. (6)

$$P_{eh,avg} = \beta_{eh} \frac{2\pi \int_0^{\pi/2} P_{eh,max} \left[2\left(\dfrac{w_{cr}}{w_{p\theta,eh}}\right) - \left(\dfrac{w_{cr}}{w_{p\theta,eh}}\right)^2 \right] \sin\theta \, d\theta}{2\pi}$$
$$= \beta_{eh} \left[\frac{2}{3} \frac{w_{cr}}{s_{eh}} - \frac{1}{5}\left(\frac{w_{cr}}{s_{eh}}\right)^2 \right] P_{eh,max} \text{ for } w_{cr} < s_{eh} \quad (6)$$

where $w_{p\theta,eh}$ is the crack width at the peak tensile force due to mechanical anchorage of a fiber with an inclination angle of θ, calculated as $w_{p\theta,eh} = s_{eh}/\cos^2\theta$; and β_{eh} is a coefficient accounting for the portion of fibers in which the tensile force due to mechanical anchorage does not reach the maximum force. In the same manner as with the derivation of β_f, it has been determined that the value of coefficient β_{eh} is 0.76. This coefficient prevents the tensile force by mechanical anchorage from being overestimated due to the effect of a fiber slip on the longer embedded side in the same manner as was done for the frictional bond behavior.

When the crack width is larger than s_{eh}, the critical fiber inclination angle corresponding to the crack width at the peak tensile force due to the mechanical anchorage can be derived as Eq. (7)

$$\theta_{crit,eh} = \cos^{-1}\left(\sqrt{s_{eh}/w_{cr}}\right) \text{ for } w_{cr} \geq s_{eh} \quad (7)$$

Therefore, as with Eq. (3), when some of the steel fibers are in the descending regime shown in Fig. 6 but no steel fiber is yet fully deteriorated, the average tensile force developed from mechanical anchorage can be calculated considering the random distribution of the fiber inclination angle as Eq. (8)

$$P_{eh,avg} = \frac{2\pi \int_0^{\theta_{crit,eh}} P_{eh,max} \left[1 - \dfrac{2\left(w_{cr} - w_{p\theta,eh}\right)}{l_f - l_i} \right] \sin\theta \, d\theta}{2\pi}$$
$$+ \frac{2\pi \int_{\theta_{crit,eh}}^{\pi/2} P_{eh,max} \left[2\left(\dfrac{w_{cr}}{w_{p\theta,eh}}\right) - \left(\dfrac{w_{cr}}{w_{p\theta,eh}}\right)^2 \right] \sin\theta \, d\theta}{2\pi} \text{ for } s_{eh} \leq w_{cr} \leq \frac{l_f - l_i}{2}$$
$$= \left[1 + \left(\frac{7\beta_{eh}}{15} - 1\right)\sqrt{\frac{s_{eh}}{w_{cr}}} - \frac{2\left(\sqrt{w_{cr}} - \sqrt{s_{eh}}\right)^2}{l_f - l_i} \right] P_{eh,max} \quad (8)$$
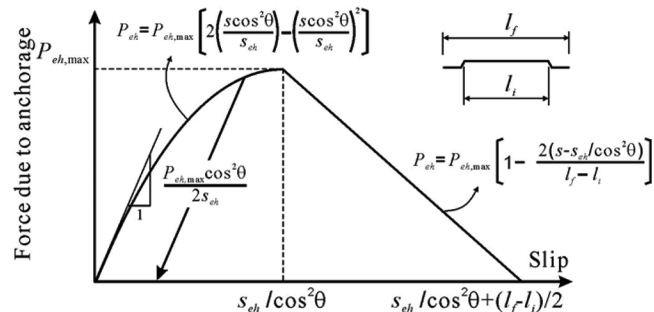

Fig. 6—Mechanical anchorage behavior in hooked-end fiber.[15]

When the crack width is sufficiently large to cause some of the end hooks to fully deteriorate by straightening or fracturing, the equation to evaluate the average tensile force due to mechanical anchorage becomes too difficult to derive exactly through integration. Therefore, a simple parabolic relationship between the crack width and the average tensile force caused by mechanical anchorage can be employed as Eq. (9)

$$P_{eh,avg} = \left(\frac{l_i - 2w_{cr}}{2l_i - l_f}\right)^2 P_{eh,avg,i} \text{ for } \frac{l_f - l_i}{2} \leq w_{cr} < \frac{l_i}{2} \quad (9)$$

where $P_{eh,avg,i}$ is the average tensile force due to the mechanical anchorage at $w_{cr} = (l_f - l_i)/2$ calculated from Eq. (8).

When the crack width is larger than $l_i/2$, it can be assumed that all mechanical anchorages have been fully exhausted.

In the calculation of the average fiber tensile stress at a crack due to the mechanical anchorage effect, the fibers in which the mechanical anchorage has pulled out should not be considered. Therefore, assuming a uniform distribution over the shorter embedment length of fibers at initial cracking, the fiber tensile stress at a crack due to the mechanical anchorage effect can be calculated as Eq. (10)

$$\sigma_{f,cr,eh} = \frac{4P_{eh,avg}}{\pi d_f^2} \frac{l_i - 2w_{cr}}{l_f} \quad (10)$$

By introducing the maximum bond strength due to the mechanical anchorage of a hooked-end fiber $\tau_{eh,max} = 2P_{eh,max}/\pi d_f l_f$ and incorporating Eq. (10) with Eq. (6), (8), and (9), the tensile stress of an SFRC element due to the mechanical anchorage effect can be calculated as Eq. (11)

$$f_{eh} = \alpha_f V_f \sigma_{f,cr,eh} = \alpha_f V_f K_{eh} \tau_{eh,max} \frac{2\left(l_i - 2w_{cr}\right)}{d_f} \quad (11)$$

where $K_{eh} = \begin{cases} \beta_{eh}\left[\dfrac{2}{3}\dfrac{w_{cr}}{s_{eh}} - \dfrac{1}{5}\left(\dfrac{w_{cr}}{s_{eh}}\right)^2\right] & \text{for } w_{cr} < s_{eh} \\[2ex] 1 + \left(\dfrac{7\beta_{eh}}{15} - 1\right)\sqrt{\dfrac{s_{eh}}{w_{cr}}} - \dfrac{2\left(\sqrt{w_{cr}} - \sqrt{s_{eh}}\right)^2}{l_f - l_i} & \text{for } s_{eh} \leq w_{cr} < \dfrac{l_f - l_i}{2} \\[2ex] \left(\dfrac{l_i - 2w_{cr}}{2l_i - l_f}\right)^2 K_{eh,i} & \text{for } \dfrac{l_f - l_i}{2} \leq w_{cr} < \dfrac{l_i}{2} \end{cases}$
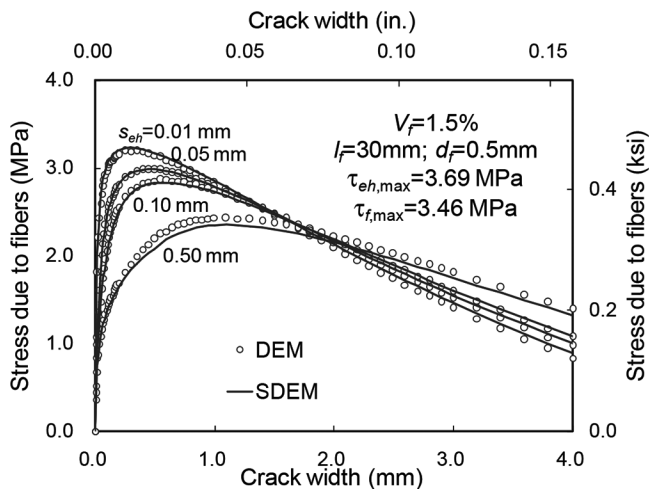
Fig. 7—Comparison of SDEM and DEM for tensile stress attained by hooked-end fibers. (Note: 1 MPa = 145 psi; 1 mm = 0.0394 in.)
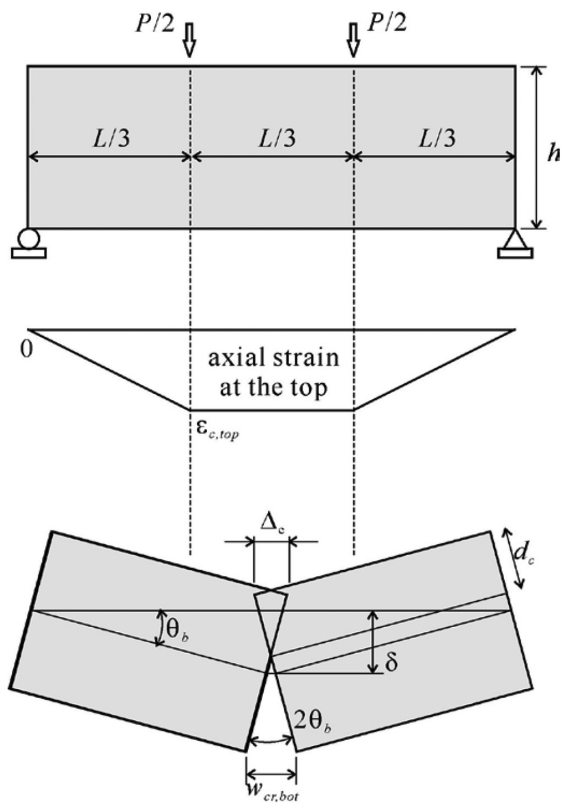

Fig. 8—Idealized failure mode of SFRC beam.[28]

where $K_{eh,i}$ is K_{eh} at $w_{cr} = (l_f - l_i)/2$.

Finally, the tensile stress attained in SFRC elements with hooked-end fibers can be calculated from the superposition of the tensile stresses due to the frictional bond behavior (Eq. (5)) and the mechanical anchorage effect (Eq. (11)). Figure 7 compares the tensile stress attained by hooked-end fibers as calculated by the DEM and SDEM. It can be seen that the results of the simplified model show good correspondence with the DEM.

Tensile stress of SFRC member

The aforementioned formulations have dealt with the tensile stress attained by steel fibers. To realistically evaluate

the tensile stress response of SFRC members, the tensile stress due to the tension-softening effect of the concrete matrix should be added to that attained by steel fibers. This study adopted the following exponential form (Eq. (12))[12] for the tension-softening effect.

$$f_{ct} = f_{cr} e^{-cw_{cr}} \tag{12}$$

where the coefficient c is 15 and 30 for concrete and mortar, respectively.

Therefore, the tensile stress of an SFRC member can be calculated as Eq. (13)

$$f_{SFRC} = f_f + f_{ct} \tag{13}$$

where f_f is the tensile stress attained by fibers, equal to f_{st} for straight fibers and $f_{st} + f_{eh}$ for hooked-end fibers.

VERIFICATION OF SDEM

As shown previously, the tensile stress response of fibers calculated by the SDEM shows good agreement with that obtained from the DEM. Because the accuracy of the DEM was validated in previous studies[15,16] through comparisons with test results involving straight[6,18] and hooked-end[6,17] fibers, it can be concluded that the structural behavior of SFRC elements subjected to direct tension can be modeled accurately by the SDEM. For further verification, plots provided in the Appendix compare the responses determined by the SDEM to the test results for several specimens. In this section, the flexural behavior of SFRC members will be discussed.

Analysis procedure for flexural behavior of SFRC members

To investigate the modeling capabilities of the SDEM for flexural members, four-point bending tests were considered. In the analysis of the flexural behavior of SFRC specimens, the sectional analysis procedure presented by Oh et al.,[28] which is useful for modeling the flexural behavior of SFRC beams exhibiting a single dominant crack, was employed. Because an SFRC beam specimen subjected to the four-point loading reaches failure through the formation of a single dominant flexural crack, the failure configuration can be assumed as Fig. 8. In this figure, the relationship between the compressive strain in the pure bending region, $\varepsilon_{c,top}$, and the center deflection, Δ_c, can be derived as Eq. (14)

$$\Delta_c = \int_0^L \varepsilon_{x,top} dx = \frac{2}{3} \varepsilon_{c,top} L \tag{14}$$

From the geometric conditions illustrated in Fig. 8, the crack opening displacement at the bottom of the beam, $w_{cr,bot}$, is $2\theta_b(h - d_c)$ and $\theta_b = \Delta_c/2d_c$. By incorporating these relationships into Eq. (14), the relationship between $\varepsilon_{c,top}$ and $w_{cr,bot}$ can be derived as Eq. (15)

$$\varepsilon_{c,top} = \frac{3}{2} \frac{d_c}{L(h - d_c)} w_{cr,bot} \tag{15}$$

With the relationship presented in Eq. (15), the strain and crack width distributions through the section at the crack location can be evaluated, as illustrated in Fig. 9(a).

The stress distribution along the uncracked depth can be evaluated for the given strain distribution. Linear (Eq. (16a)) and parabolic (Eq. (16b)) relationships[29] can be employed for the post- and pre-peak compressive behavior, respectively, while a linear relationship (Eq. (16c)) can be used for the tensile behavior before cracking, as illustrated in Fig. 10.

$$f_c = f_c' \left[1 - \frac{0.15}{0.004 - \varepsilon_o} (\varepsilon_c - \varepsilon_o) \right] \text{ for } \varepsilon_c < \varepsilon_o \quad (16a)$$

$$f_c = f_c' \left[2 \frac{\varepsilon_c}{\varepsilon_o} - \left(\frac{\varepsilon_c}{\varepsilon_o} \right)^2 \right] \text{ for } \varepsilon_o \le \varepsilon_c < 0 \quad (16b)$$

$$f_c = \varepsilon_c E_c \text{ for } 0 \le \varepsilon_c < \varepsilon_{cr} \quad (16c)$$

where $\varepsilon_o = 2f_c'/E_c$ and $E_c = 3300\sqrt{f_c'} + 6900$ (Reference 30) because the inclusion of steel fibers has only a minor influence on the initial elastic modulus in specimens where the casting direction is parallel to the crack surface.[31] The tensile stress within the cracked zone can be evaluated for a given crack width distribution using Eq. (5) and (11) through (13).

Consequently, the sectional analysis for a section containing a flexural crack can be conducted through an iteration procedure, finding the depth of the neutral axis for a given crack opening width at the bottom of the section by satisfying equilibrium for the horizontal force. Then, the sectional moment M can be calculated from the stress distribution through the depth of the section. Finally, the applied force and the center deflection can be calculated as Eq. (17) and (18)

$$P = \frac{6M}{L} \quad (17)$$

$$\delta = \theta_b \frac{L}{2} = \frac{L}{4(h - d_c)} w_{cr,bot} \quad (18)$$

Comparison with test results of SFRC members

As a verification of the SDEM, both the direct tensile and the flexural specimens tested by Susetyo[17] will be analyzed. In these tests, the cross section of the direct tension test specimens was 70 x 100 mm^2 (2.8 x 3.9 in.^{2}) and the dimensions of the flexural test specimens were 152 (b) x 152 (h) x 456 (L) mm^3 (6.0 x 6.0 x 18.0 in.^{3}). The test variables included the fiber volumetric ratio, fiber aspect ratio (l_f/d_f), and concrete compressive strength. When the SDEM was employed to evaluate the tensile stress attained by steel fibers, the slips corresponding to the bond strength due to the frictional bond behavior, s_f, and the maximum force due to the mechanical anchorage, s_{eh}, were assumed to be 0.01 and 0.1 mm (0.0004 and 0.004 in.), respectively, as suggested by Naaman and Najm.[10] The frictional bond strength $\tau_{f,max}$ and the mechanical anchorage strength $\tau_{eh,max}$ were assumed to be
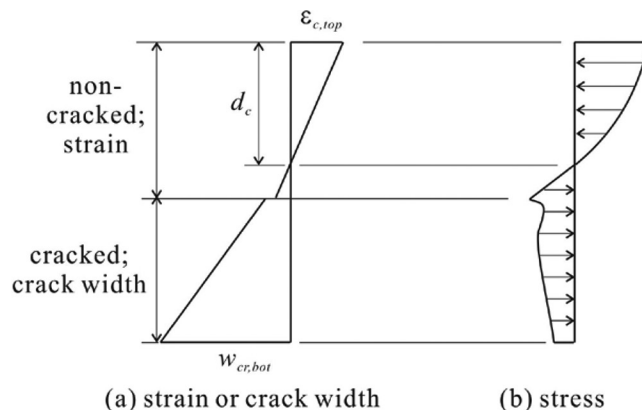

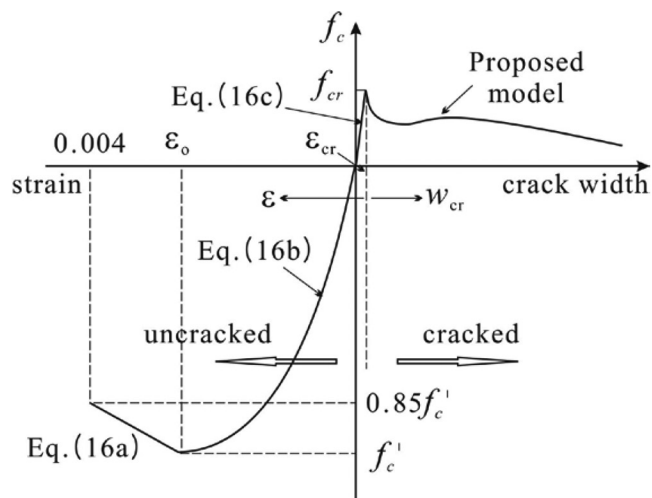Fig. 9—Crack width, strain, and stress distribution through section.

Fig. 10—Material model for SFRC.

$0.396\sqrt{f_c'}$ and $0.429\sqrt{f_c'}$ in MPa ($4.77\sqrt{f_c'}$ and $5.17\sqrt{f_c'}$ in psi), respectively, based on previous studies.[12,16] Because the elastic deformation of the uncracked region of the beam is ignored in the assumed failure mode, the analysis was conducted starting with a 0.5 mm (0.02 in.) crack opening width at the bottom of the cracked section. Note that the SFRC beams used for the verification study exhibited a single dominant flexural crack. As shown in Fig. 11 and 12, the analysis results obtained from the SDEM show good agreement with the test results of the SFRC members, not only with the direct tensile behavior but also with the flexural behavior.

CONCLUSIONS

In this paper, a simplified version of the DEM was developed by eliminating the double numerical integration procedure. To enable the simplification, it was assumed that the fiber slip on the shorter embedded side is the same as the crack width. As a result, the fiber tensile stress at a crack can be calculated directly for a given crack width by considering the same constitutive models for frictional bond behavior and the mechanical anchorage effect, as employed in the DEM for the pullout behavior of a single fiber embedded on both sides. To prevent an overestimation of the fiber tensile stress at a crack that could be caused by neglecting the
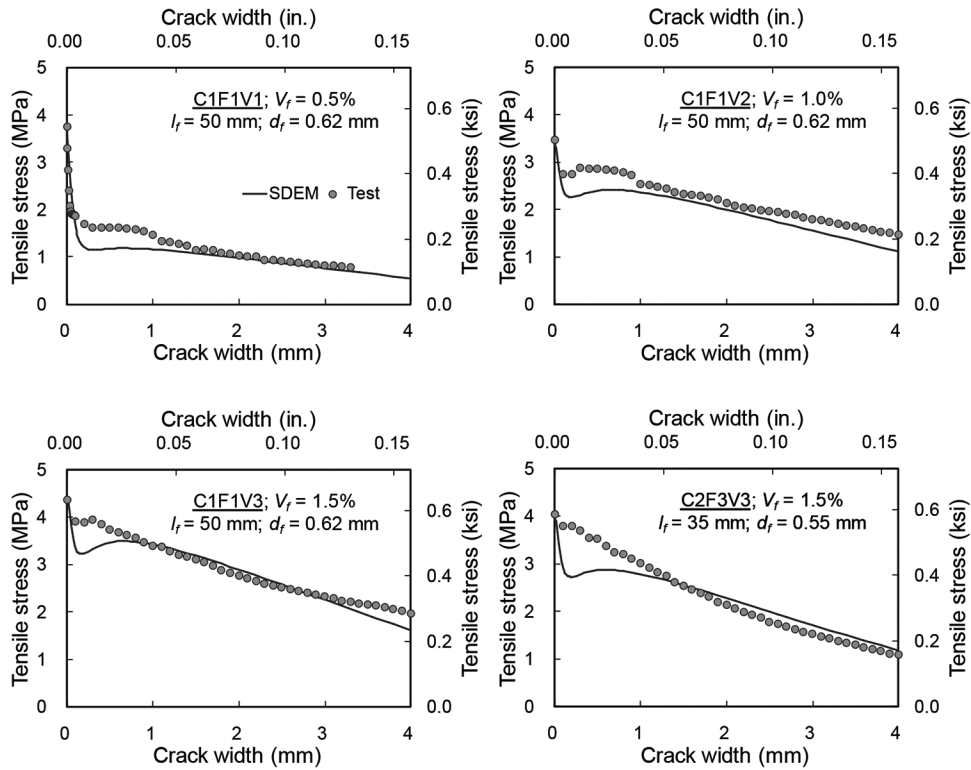
Fig. 11—Comparison of tensile behavior of SFRC members with hooked-end fibers tested by Susetyo.[17] (Note: 1 mm = 0.0394 in.)
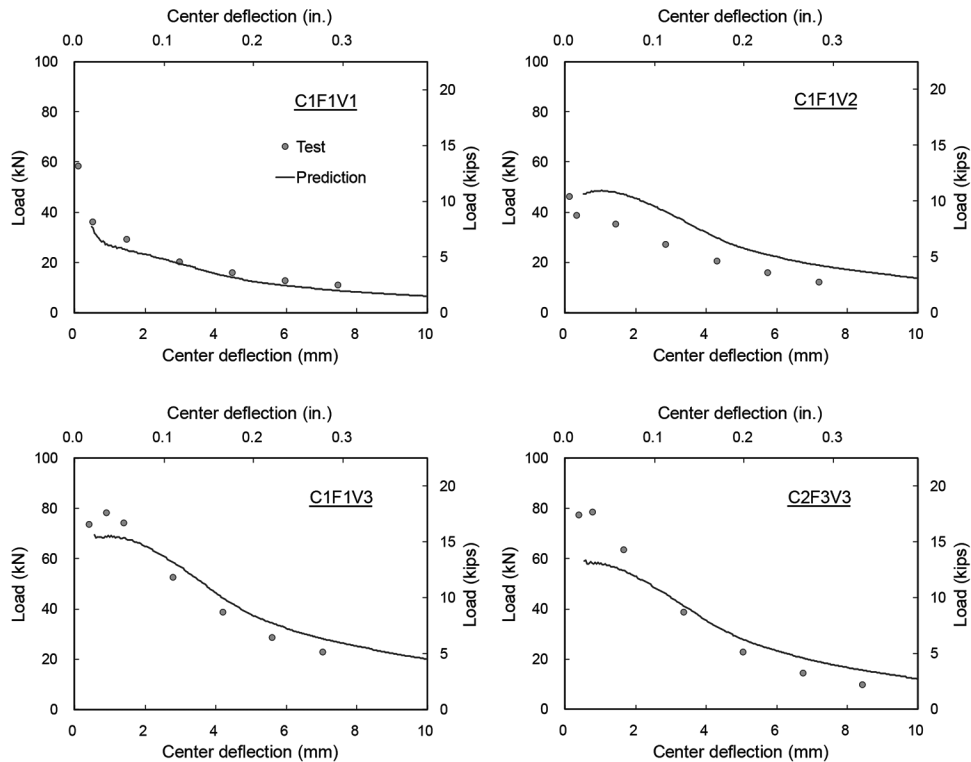

Fig. 12—Comparison of flexural behavior of SFRC beams tested by Susetyo.[17]

effect of a fiber slip on the longer embedded side, the coefficients β_f and β_{eh} were introduced for the frictional bond behavior and the mechanical anchorage effect, respectively. Consequently, the tensile stress attained by fibers in SFRC members can be more simply evaluated.

The accuracy of the SDEM was verified through the analysis of various test specimens. The tensile stress responses of steel fibers calculated by the SDEM showed good agreement with those obtained from the DEM. This was true regardless of the pullout characteristics of a fiber,

such as the slips corresponding to the maximum fiber tensile stress due to the frictional bond behavior and the mechanical anchorage effect, respectively. In comparisons with test results, the SDEM predicted the direct tensile behavior of SFRC members with straight fibers or hooked-end fibers well. From sectional analyses with pre-assumed failure modes, the SDEM also showed good agreement with the test results for the flexural behavior of SFRC beams. Consequently, it can be concluded that the tensile or flexural behavior of SFRC members can be modeled simply and accurately with the SDEM.

The proposed SDEM can be easily implemented into currently available analysis models[19-22] or programs[23,24] so that it can be useful in the assessment of the structural behavior of SFRC members or structures with or without conventional reinforcing bars.

NOTATION

A_f	=	cross-sectional area of fiber
b, h	=	width and height of rectangular cross section, respectively
c	=	coefficient for tension-softening effect of concrete or mortar
d_c	=	depth to neural axis from top surface
d_f	=	fiber diameter
E_c	=	Young's modulus of concrete
f_c	=	concrete stress at uncracked depth
f_c'	=	concrete compressive strength
f_{cr}	=	cracking strength of concrete or mortar matrix
f_{ct}	=	tensile stress by concrete/mortar tension softening at given crack width
f_f	=	tensile stress attained by steel fibers
f_{SFRC}	=	total tensile stresses of SFRC member
f_{st}, f_{eh}	=	tensile stresses attained by fibers due to frictional bond behavior and mechanical anchorage effect, respectively
$K_{eh,i}$	=	K_{eh} at $w_{cr} = (l_f - l_i)/2$
K_f	=	bond modulus, which is slope for elastic behavior in bond stress-slip relationship for fiber
K_{st}, K_{eh}	=	factors to represent average pullout stresses of fiber due to frictional bond behavior and mechanical anchorage of hooked-end fiber, respectively
L	=	clear span of beam
l_f	=	fiber length
l_i	=	distance between mechanical anchorages for hooked-end fiber
M	=	applied moment in pure bending region
P	=	applied force in beam
$P_{eh,avg}$, $P_{eh,max}$	=	average and maximum tensile force due to mechanical anchorage of hooked-end fiber, respectively
$P_{eh,avg,i}$	=	$P_{eh,avg}$ at $w_{cr} = (l_f - l_i)/2$
s_{eh}	=	slip at maximum tensile force due to mechanical anchorage of fiber with inclination angle of 0 degrees to normal of crack surface
s_f	=	slip at frictional bond strength for fiber with inclination angle of 0 degrees
V_f	=	fiber volumetric ratio
w_{cr}	=	crack width
$w_{cr,bot}$	=	flexural crack width at bottom of beam
$w_{p\theta,eh}$	=	crack width at peak tensile force due to mechanical anchorage of fiber with inclination angle of θ
$w_{p\theta,f}$	=	crack width at initiation of plastic frictional bond behavior of fiber with inclination angle of θ
x	=	distance from support
α_f	=	fiber orientation factor
β_f, β_{eh}	=	coefficients to consider effect of fiber slip on longer embedment side on frictional behavior and mechanical anchorage effect, respectively
Δ_c	=	compressive deformation at top surface in pure bending region
δ	=	deflection of beam at cracked section
ε_c	=	concrete strain at uncracked depth
$\varepsilon_{c,top}$	=	compressive strain at top of section in pure bending region
ε_o	=	compressive strain at f_c'
$\varepsilon_{x,top}$	=	compressive strain at top of section at distance of x from support
θ	=	fiber inclination angle from axis perpendicular to crack surface
θ_b	=	rotation angle of cracked beam
$\theta_{crit,f}$, $\theta_{crit,eh}$	=	fiber inclination angles corresponding to pullout strengths due to frictional bond behavior and mechanical anchorage effect, respectively
$\sigma_{f,cr,st}$, $\sigma_{f,cr,eh}$	=	average fiber stresses at crack due to frictional bond behavior and mechanical anchorage effect, respectively
$\tau_{eh,max}$	=	pullout strength due to mechanical anchorage of hooked-end fiber
$\tau_{f,avg}$	=	average frictional bond stress
$\tau_{f,max}$	=	frictional bond strength

REFERENCES
1. Parra-Montesinos, G. J., "High-Performance Fiber-Reinforced Cement Composites: An Alternative for Seismic Design of Structures," *ACI Structural Journal*, V. 102, No. 5, Sept.-Oct. 2005, pp. 668-675.

2. Minelli, F., and Vecchio, F. J., "Compression Field Modeling of Fiber-Reinforced Concrete Members under Shear Loading," *ACI Structural Journal*, V. 103, No. 2, Mar.-Apr. 2006, pp. 244-252.

3. Dinh, H. H.; Parra-Montesinos, G. J.; and Wight, J. K., "Shear Behavior of Steel Fiber-Reinforced Concrete Beams without Stirrup Reinforcement," *ACI Structural Journal*, V. 107, No. 5, Sept.-Oct. 2010, pp. 597-606.

4. Susetyo, J.; Gauvreau, P.; and Vecchio, F. J., "Effectiveness of Steel Fiber as Minimum Shear Reinforcement," *ACI Structural Journal*, V. 108, No. 4, July-Aug. 2011, pp. 488-496.

5. Petersson, P. E., "Fracture Mechanical Calculations and Tests for Fiber-Reinforced Concrete in Tension," *Proceedings of Advances in Cement-Matrix Composites*, Materials Research Society, Boston, MA, 1980, pp. 95-106.

6. Lim, T. Y.; Paramasivam, P.; and Lee, S. L., "Analytical Model for Tensile Behavior of Steel-Fiber Concrete," *ACI Materials Journal*, V. 84, No. 4, July-Aug. 1987, pp. 286-298.

7. Li, Z.; Li, F.; Chang, T.-Y. P.; and Mai, Y.-W., "Uniaxial Tensile Behavior of Concrete Reinforced with Randomly Distributed Short Fibers," *ACI Materials Journal*, V. 95, No. 5, Sept.-Oct. 1998, pp. 564-574.

8. Groth, P., "Fibre Reinforced Concrete—Fracture Mechanics Methods Applied on Self-Compacting Concrete and Energetically Modified Binders," doctoral thesis, Department of Civil and Mining Engineering, Division of Structural Engineering, Luleå University of Technology, Luleå, Sweden, 2000, 237 pp.

9. Barragán, B. E.; Gettu, R.; Martín, M. A.; and Zerbino, R. L., "Uniaxial Tension Test for Steel Fibre Reinforced Concrete—A Parametric Study," *Cement and Concrete Composites*, V. 25, No. 7, Oct. 2003, pp. 767-777.

10. Naaman, A. E., and Najm, H., "Bond-Slip Mechanisms of Steel Fibers in Concrete," *ACI Materials Journal*, V. 88, No. 2, Mar.-Apr. 1991, pp. 135-145.

11. Marti, P.; Pfyl, T.; Sigrist, V.; and Ulaga, T., "Harmonized Test Procedures for Steel Fiber-Reinforced Concrete," *ACI Materials Journal*, V. 96, No. 6, Nov.-Dec. 1999, pp. 676-686.

12. Voo, J. Y. L., and Foster, S. J., "Variable Engagement Model for Fibre Reinforced Concrete in Tension," *Univiv Report No. R-420*, School of Civil and Environmental Engineering, the University of New South Wales, Sydney, NSW, Australia, June 2003, 86 pp.

13. Leutbecher, T., and Fehling E., "Crack Width Control for Combined Reinforcement of Rebars and Fibers Exemplified by Ultra-High-Performance Concrete," *fib* Task Group 8.6, Ultra High Performance Fiber Reinforced Concrete—UHPFRC, Sept. 2008, pp. 1-28.

14. Stroeven, P., "Stereological Principles of Spatial Modeling Applied to Steel Fiber-Reinforced Concrete in Tension," *ACI Materials Journal*, V. 106, No. 3, May-June 2009, pp. 213-222.

15. Lee, S.-C.; Cho, J.-Y.; and Vecchio, F. J., "Diverse Embedment Model for Steel Fiber-Reinforced Concrete in Tension: Model Development," *ACI Materials Journal*, V. 108, No. 5, Sept.-Oct. 2011, pp. 516-525.

16. Lee, S.-C.; Cho, J.-Y.; and Vecchio, F. J., "Diverse Embedment Model for Steel Fiber-Reinforced Concrete in Tension: Model Verification," *ACI Materials Journal*, V. 108, No. 5, Sept.-Oct. 2011, pp. 526-535.

17. Susetyo, J., "Fibre Reinforcement for Shrinkage Crack Control in Prestressed, Precast Segmental Bridges," doctoral thesis, Department of

Civil Engineering, University of Toronto, Toronto, ON, Canada, 2009, 307 pp.

18. Petersson, P. E., "Fracture Mechanical Calculations and Tests for Fiber-Reinforced Cementitious Materials," *Proceedings of Advances in Cement-Matrix Composites*, Materials Research Society, Boston, MA, 1980, pp. 95-106.

19. Vecchio, F. J., and Collins, M. P., "The Modified Compression Field Theory for Reinforced Concrete Elements Subjected to Shear," *ACI Journal*, V. 83, No. 2, Mar.-Apr. 1986, pp. 219-231.

20. Vecchio, F. J., "Disturbed Stress Field Model for Reinforced Concrete: Formulation," *Journal of Structural Engineering*, ASCE, V. 126, No. 9, Sept. 2000, pp. 1070-1077.

21. Vecchio, F. J., "Disturbed Stress Field Model for Reinforced Concrete: Implementation," *Journal of Structural Engineering*, ASCE, V. 127, No. 1, Jan. 2001, pp. 12-20.

22. Lee, S.-C.; Cho, J.-Y.; and Vecchio, F. J., "Tension-Stiffening Model for Steel Fiber-Reinforced Concrete Containing Conventional Reinforcement," *ACI Structural Journal*, V. 110, No. 4, July-Aug. 2013, pp. 639-648.

23. Bentz, E. C., "Sectional Analysis of Reinforced Concrete Members," doctoral thesis, Department of Civil Engineering, University of Toronto, Toronto, ON, Canada, 2000, 184 pp.

24. Wong, P. S., and Vecchio, F. J., "VecTor2 & FormWorks User's Manual," *Publication* No. 2002-02, Department of Civil Engineering, University of Toronto, Toronto, ON, Canada, Aug. 2002, 214 pp.

25. Banthia, N., and Trottier, J.-F., "Concrete Reinforced with Deformed Steel Fibers, Part I: Bond-Slip Mechanisms," *ACI Materials Journal*, V. 91, No. 5, Sept.-Oct. 1994, pp. 320-348.

26. Soroushian, P., and Lee, C.-D., "Distribution and Orientation of Fibers in Steel Fiber Reinforced Concrete," *ACI Materials Journal*, V. 87, No. 5, Sept.-Oct. 1990, pp. 433-439.

27. Sujivorakul, C.; Waas, A. M.; and Naaman, A. E., "Pullout Response of a Smooth Fiber with an End Anchorage," *Journal of Engineering Mechanics*, ASCE, V. 126, No. 9, Sept. 2000, pp. 986-993.

28. Oh, B. H.; Park, D. G.; Kim, J. C.; and Choi, Y. C., "Experimental and Theoretical Investigation on the Postcracking Inelastic Behavior of Synthetic Fiber Reinforced Concrete Beams," *Cement and Concrete Research*, V. 35, No. 2, Feb. 2005, pp. 384-392.

29. Park, R., and Pauley, T., *Reinforced Concrete Structures*, John Wiley & Sons, Inc., New York, 1975, 769 pp.

30. CSA A23.3-04, "Design of Concrete Structures," Canadian Standards Association, Mississauga, ON, Canada, 2004, 214 pp.

31. Mansur, M. A.; Chin, M. S.; and Wee, T. H., "Stress-Strain Relationship of High-Strength Fiber Concrete in Compression," *Journal of Materials in Civil Engineering*, ASCE, V. 11, No. 1, Feb. 1999, pp. 21-29.

Appendix

Note: 'Proposed' in Figs. A1-A4 represents predictions made with the SDEM developed in this paper.; The predictions of SDEM overlap with those of DEM developed by Lee et al.[15-16] for almost all specimens.; All analytical predictions do not consider member dimension.
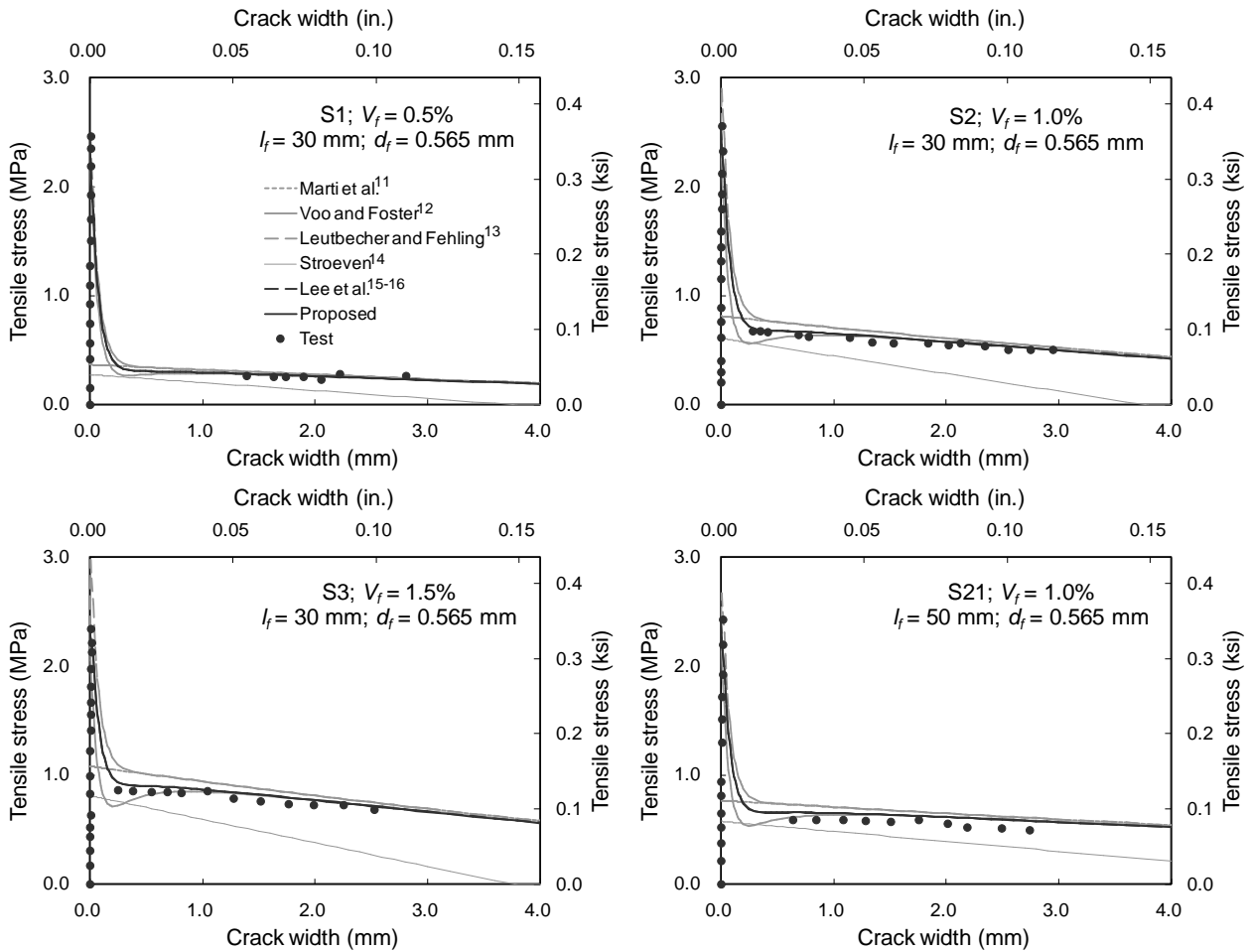

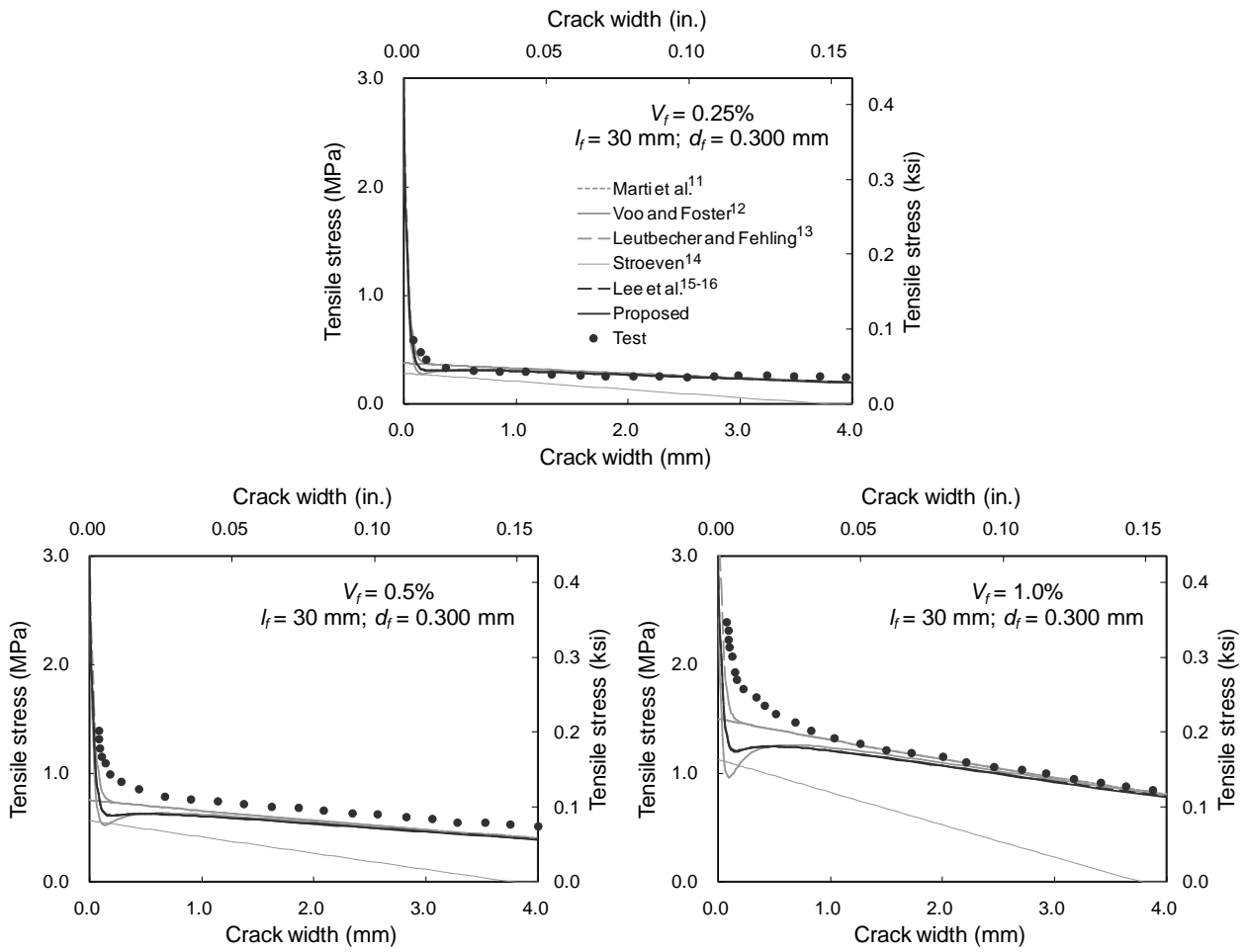Fig. A1. Comparison with test results for members with straight fibers tested by Lim et al.[6]

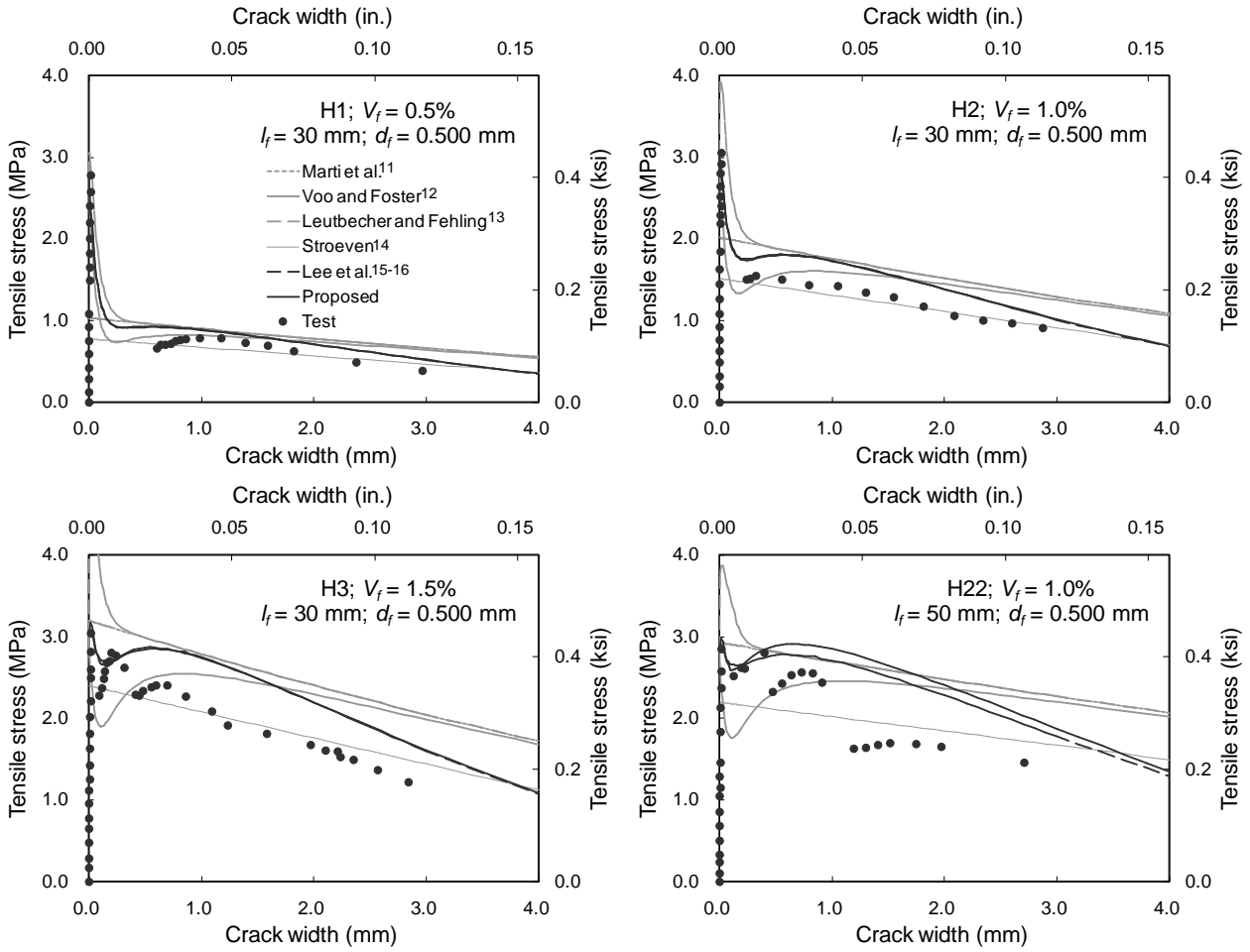Fig. A2. Comparison with test results for members with straight fibers tested by Petersson[18]

Fig. A3. Comparison with test results for members with end-hooked fibers tested by Lim et al.[6]
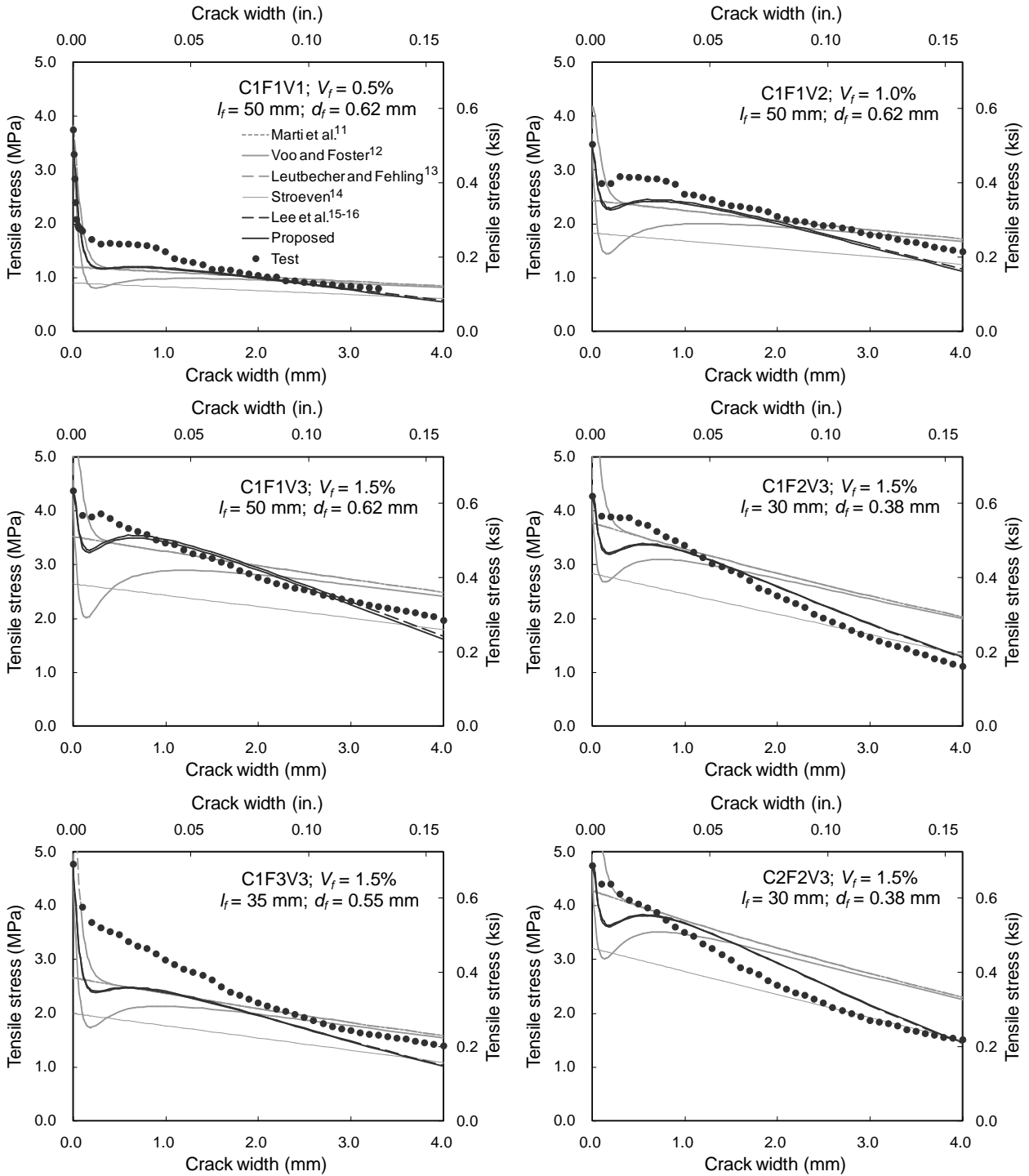
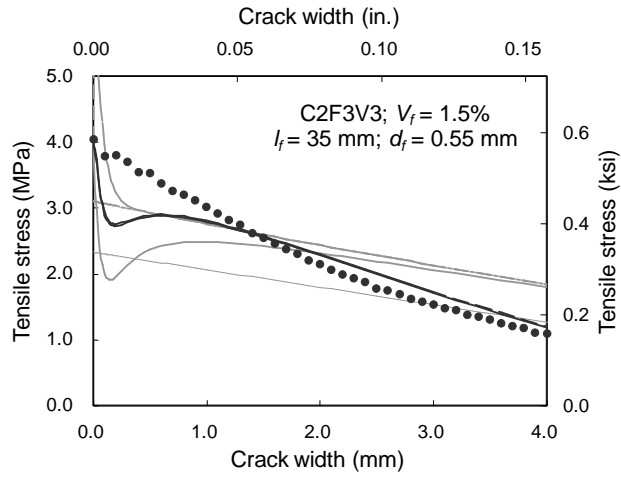Fig. A4. Comparison with test results for members with end-hooked fibers tested by Susetyo[17]

Fig. A4. Comparison with test results for members with end-hooked fibers tested by Susetyo[17] (continued)